frontiers | Frontiers in Thermal Engineering

TYPE Original Research
PUBLISHED 16 January 2023
DOI 10.3389/fther.2022.1079789

OPEN ACCESS

EDITED BY
Boxiang Wang,
Shanghai Jiao Tong University, China

REVIEWED BY
Fan Zhang,
Tianjin University, China
Milan S. Dimitrijevic,
Astronomical Observatory, Serbia

*CORRESPONDENCE
Tanvir I. Farouk,
tfarouk@sc.edu

SPECIALTY SECTION
This article was submitted to Heat Transfer Mechanisms and Applications, a section of the journal Frontiers in Thermal Engineering

RECEIVED 25 October 2022
ACCEPTED 06 December 2022
PUBLISHED 16 January 2023

CITATION
Ahmed SF, Aghdam AC, Pleis J, Geiger R and Farouk TI (2023), Electric field assisted reduction of NO_x emission: A numerical study.
Front. Front. Therm. Eng. 2:1079789.
doi: 10.3389/fther.2022.1079789

Electric field assisted reduction of NO_x emission: A numerical study

Sheikh F. Ahmed[1], Ali Charchi Aghdam[1], Jackson Pleis[2], Robert Geiger[2] and Tanvir I. Farouk[1]*

[1]Department of Mechanical Engineering, University of South Carolina, Columbia, SC, United States, [2]ClearSign Combustion Corporation, Seattle, WA, United States

The paper reports simulation results on the influence of a direct-current driven radial electric field on the emission characteristics; especially NO_x and CO of a premixed methane/air laminar jet flame. A multi-physics computational model is developed in the OpenFOAM framework to simulate electric-field-coupled premixed combustion process. The computational framework consists of coupled species, momentum and energy conservation together with a Poisson's equation solver to resolve the electric field distribution. Electron and ion conservation equations are resolved to consider the ionic wind body force in the momentum conservation equation and the associated possible electric field distortion due to the space charge distribution. The simulations are conducted for a stochiometric and fuel rich condition and over a range of jet flow rates for a configuration representative of a test-scale experimental setup. The model predictions show that for an applied voltage of 50 kV, the flame structure changes significantly for both the stoichiometric and fuel rich conditions. The flame is stretched significantly by the electric field due to ionic wind. For the fuel rich condition, the ionic wind allows additional mixing of the fuel rich stream with the surrounding air and drastically altering the flame structure. The electric field was found to reduce the NO_x emission significantly for both stoichiometric and rich conditions. Over the entire range of flowrate conditions, the stochiometric fuel-oxidizer mixture showed a decrease in maximum NO_x by a factor of 1.6 in presence of electric field. For the fuel rich case, however as the flow rate is increased, the NO_x reduction factor decreased from 12.0 to 1.6. For CO emissions, the presence of electric field reduces the concentration under fuel rich conditions and *vice versa* for the stoichiometric flame. The role of kinetics is analyzed and discussed.

KEYWORDS

chemi-ionization, electric field, ionic wind, NO_x kinetics, OpenFOAM

1 Introduction

For several decades, researchers have been interested in the electrical properties of flames and how they can be controlled by the application of electric fields. It has been shown that electric fields affect flames and combustion processes in three distinctive, and major ways–thermal effect (Uddi et al., 2009), ionic wind effect (Marcum and Ganguly, 2005), and electro-chemical effect (Ombrello et al., 2010a,b). The thermal effect contributes to the neutral gas heating through Joule heating when there is large current across the electric field. The ionic wind effect causes fluid dynamic changes in the flow field via electrical body force resulting from space charge and electric field. The electro-chemical effect produces energetic electrons, ions, radicals and excited molecules in the gas stream which directly contributes to the reaction kinetics.

Studies involving experimental and modeling approaches have been conducted, in an effort to elucidate the influence of both direct-current (DC) and alternating-current (AC) electric fields on the combustion characteristics. Experimental studies have demonstrated that DC electric fields have a strong influence on the flame shape (Vega et al., 2007), flame propagation speed (Marcum and Ganguly, 2005), and emission and soot characteristics (Saito et al., 1999; Sakhrieh et al., 2005). Simulations employing multi-physics models have shown the role of ionic wind under DC external fields (Yamashita et al., 2009; Belhi et al., 2010; Belhi et al., 2019). In recent years, there has been growing interest in utilizing AC electric field to modify the combustion characteristics of flames (Zhang et al., 2013; Kim et al., 2017). Despite the large volume of work on electric field–flame interactions, studies related to the impact of electric field on NO_x emission is limited. Vatazhin et al. (1995) in their laminar propane diffusion flame experiments observed up to 30% reduction in NO_x emission with respect to the emission index with the implementation of electric field on a negatively polarized burner. Zake et al. (2000) applied a DC electric field in a flame channel flow and observed a reduction in the NO_x emission by ~ 80%. The decrease in the emission characteristics was attributed to the reduction in the flame temperature in presence of the electric field. Sakhrieh et al. (2005) experimentally investigated the influence of electric field on premixed methane/air flames at elevated pressures. They observed as much as 95% reduction of CO emission, accompanied by 25% increase of NO_x irrespective of pressure. They attributed the decrease in CO to ionic winds that changed the flame geometry and reduced the amount of incompletely burned fuel. However, explanation related to the increase in NO_x was not provided. In their experimental work, Vega et al. (2007) showed that for a premixed $CH_4/O_2/N_2$ flame, the NO_x emission is unaffected under applied electric field conditions for which the flame remains undeformed. In a recent paper, Zhang et al. (2013) examined the behavior of NO emission of laminar non-premixed CH_4/air flame when subjected to high frequency (10 kHz) AC electric fields. For a voltage range of 0–4.0 kV, a non-linear response of NO emission was observed. In between 0–1 kV peak voltage, the NO in flue gas showed a sharp decrease which then steadily increased to high values for 1.0–3.0 kV, followed by a steady decrease by further increase of the applied peak potential to 4 kV.

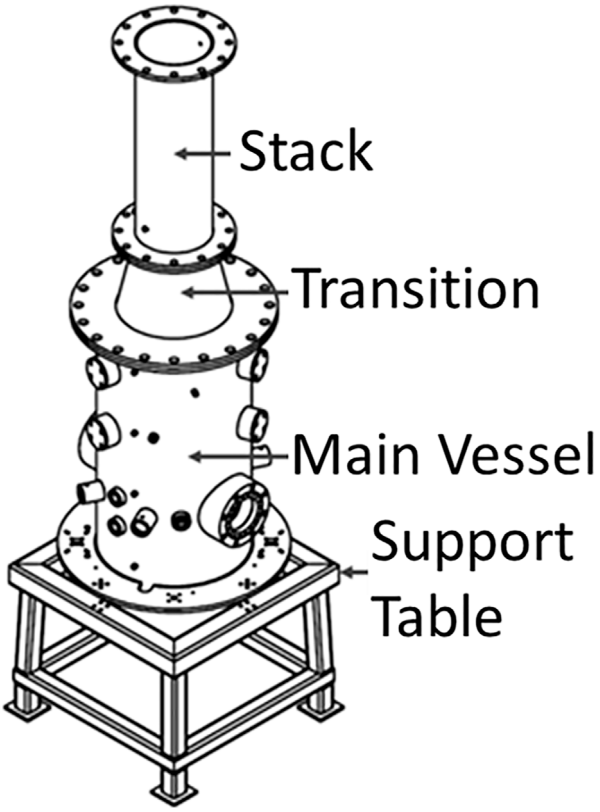

FIGURE 1
Customized test furnace for testing electric field effects on combustion process (burner assembly not shown).

In this paper, we numerically investigate the effects of an externally driven radial DC electric field on the flame and combustion characteristics, more specifically on the NO_x and CO emission in a laminar premixed CH_4/air jet flame under atmospheric condition. The simulation was conducted for a multi-dimensional configuration representative of a laboratory scale mockup of an industrial system at ClearSign Combustion Corporation. A stochiometric and fuel-rich condition is investigated. The flame structure is analyzed, and the role of underlying thermo-kinetic/transport properties on emission characteristics is elucidated. The kinetic analysis shows that the NO_x recycling pathways undergo distinct changes in presence of the external fields.

2 Methods

A custom test furnace was designed and built to study the effects of electric fields on the combustion process. The furnace was designed to operate up to 5.86 kW at temperatures up to 1366 K. As shown in Figure 1, the furnace consists of a main vessel, a transition, a stack, and a burner assembly (not shown in figure). The main vessel is 1.37 m tall and has an outer diameter of 0.61 m. It contains a 0.152 m thick refractory resulting in an inner opening diameter of 0.3048 m. The transition piece is 0.360 m tall and takes the 0.61 m outer diameter of the main vessel down to a 0.305 m to match the outer diameter of the stack. The main vessel sits on four standoff electrical insulators capable of withstanding up to 50 kV. The support stand is kept at ground potential, while the rest of the vessel is electrically floating. To monitor the floating voltage of the cooling jackets and the main vessel, and to protect from large over voltages, the voltage of each is monitored through a voltage divider circuit connected to a spark gap. The spark gap can be adjusted to the desired allowable maximum voltage. The output of the voltage divider is monitored through the data acquisition system. The main vessel has two gated 0.15 m quartz windows and four 0.051 m viewing ports all on the same plane. There is a total of 26 K-type thermocouples located throughout the furnace to measure the temperatures of vessel wall and axis, cooling jackets and the top and bottom of the stack. Fuel and air are monitored using FMA 2300 series omega mass flow meters. NO_x, CO and CO_2 emission analyzers allow assessment of emission in the stacks.

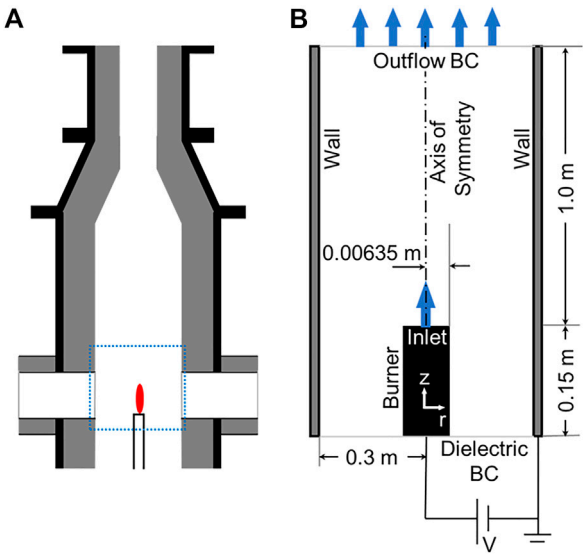

FIGURE 2
Schematic illustrations of **(A)** the experimental setup and, **(B)** the computational domain denoting the different boundaries.

2.1 Computational domain and boundary conditions

A schematic of the experimental test scale setup at ClearSign Combustion Corporation is presented in Figure 2A. The computational domain illustrated in Figure 2B takes into account only the burner and part of the post-combustion zone of the experimental setup. The domain contains part of the burner height (i.e., 0.15 m) and covers a 1.0 m long post-combustion zone having a constant diameter of 0.6 m. To reduce computational overhead, the simulations are performed on a 2-D axisymmeteric configuration with structured non-uniform mesh. The mesh was finer near the central region (i.e., jet location) as well as near the wall boundaries. All the simulations reported here are for a domain composed of 10,850 mesh elements for which grid independent results were confirmed.

The burner acts as the powered electrode (50 kV for base case simulations) with the side walls grounded (0 kV). Both are prescribed with an isothermal (i.e., 300 K) boundary conditions. The side walls and the burner surfaces are considered to be reactively non-participating for the neutral species, but the ionic species reaching the surfaces are prescribed to undergo quenching/neutralization reactions (Farouk et al., 2006). A Dirichlet boundary condition for velocity is employed at the inlet, representing the different flow rate conditions considered. Outflow boundary conditions are provided at the outlet of the tubular section. Premixed methane/air mixtures at equivalence ratios ϕ = 1.0 and 3.0, and flowrates ~ 6.70 and 9.93 slpm, respectively are simulated. An initial high temperature region of 2100 K is prescribed to ensure ignition of the fuel/air mixture. All simulations are conducted for an operating pressure of 1 atm.

2.2 Mathematical model

The numerical study is performed using a multi-dimensional, reacting flow computational code that has been developed in the OpenFOAM framework, the details of which (both the physics and the numerical schemes) have been thoroughly presented in Asgari et al., 2017 and Ahmed et al., 2021. As a new implementation, the CVODE solver from SUNDIAL is employed to solve the reaction terms. In brief, the mathematical model comprises of time dependent conservation equations of total mass, species mass fraction, mixture momentum, and mixture energy, together with a Poisson's equation to resolve the electric field distribution, reported respectively in the following:

$$\frac{\partial \rho}{\partial t} + \frac{\partial (\rho u_i)}{\partial x_i} = 0, \tag{1}$$

$$\frac{\partial (\rho Y_k)}{\partial t} + \frac{\partial}{\partial x_i}(\rho u_i Y_k) + \frac{\partial}{\partial x_i}(q_k \rho \mu_k Y_k E_i) + \frac{\partial}{\partial x_i}(\rho W_{k,i} Y_k) + \frac{\partial}{\partial x_i}(\rho V_i^c Y_k) = \dot{\omega}_k + \frac{\partial}{\partial x_i}\left(\rho D_{km} \frac{\partial Y_k}{\partial x_i}\right), \tag{2}$$

$$\frac{\partial (\rho u_i)}{\partial t} + \frac{\partial (\rho u_i u_j)}{\partial x_i} = -\delta_{ij}\frac{\partial P}{\partial x_j} + \mu \frac{\partial}{\partial x_j}\left(\frac{\partial u_i}{\partial x_j} + \frac{\partial u_j}{\partial x_i}\right) - \frac{2}{3}\mu \delta_{ij}\frac{\partial}{\partial x_j}\left(\frac{\partial u_m}{\partial x_m}\right) + q E_i, \tag{3}$$

$$\frac{\partial (\rho h_s)}{\partial t} + \frac{\partial}{\partial x_j}(\rho u_j h_s) + \frac{\partial (\rho K)}{\partial t} + \frac{\partial}{\partial x_j}(\rho u_j K) = \frac{\partial}{\partial x_j}\left(\rho \alpha \frac{\partial h_s}{\partial x_j}\right) - \frac{\partial}{\partial x_j}\left(\rho \alpha \sum_{k=1}^{N} h_{s,k} \frac{\partial Y_k}{\partial x_j}\right) + \frac{\partial P}{\partial t} + \dot{Q} + \frac{\partial}{\partial x_j}(\sigma_{ij} u_i) - \frac{\partial}{\partial x_j}\left(\rho \sum_{k=1}^{N} h_{s,k} Y_k V_{k,j}\right) - \sum_{k=1}^{N} \dot{\omega}_k \Delta h_{f,k}^0, \tag{4}$$

$$\nabla.(\varepsilon \nabla \Phi) = q_0 \sum Z_k N_k, \quad E = -\nabla \Phi, \tag{5}$$

where, ρ is the mixture density of gas phase, u is the velocity, $\dot{\omega}_k$ is the rate of productions (ROP) of species k by chemical reaction, $W_{k,i}$ is the thermophoretic diffusion velocity which is neglected in the present investigation, V_i^C is the correction velocity to ensure that the diffusion velocities of all the species add up to zero, D_{km} is the mass diffusion coefficient of species k into the rest of the mixture, P is the pressure, h_s is the specific enthalpy of species k, α is the mixture thermal diffusivity, $\Delta h_{f,k}^o$ is the formation enthalpy for species k, $\dot{Q}$ is the energy source term due to radiation, Φ is the electric potential, ε is the electric permittivity, q_0 is the elementary charge, Z_k is the electric charge of species k, and N_k is the number density of species k. The momentum conservation includes the effect of electrical body force i.e., $q.\vec{E}$. Conservation equation for both electrons and ions are solved including the effect of drift velocity ($v_{\text{drift}} = \mu_{\text{mobility}}\vec{E}$) of the ionic species. Even though electrons are included in the computation, their effect on the system is not significant due to their very low number density and extremely high mobility.

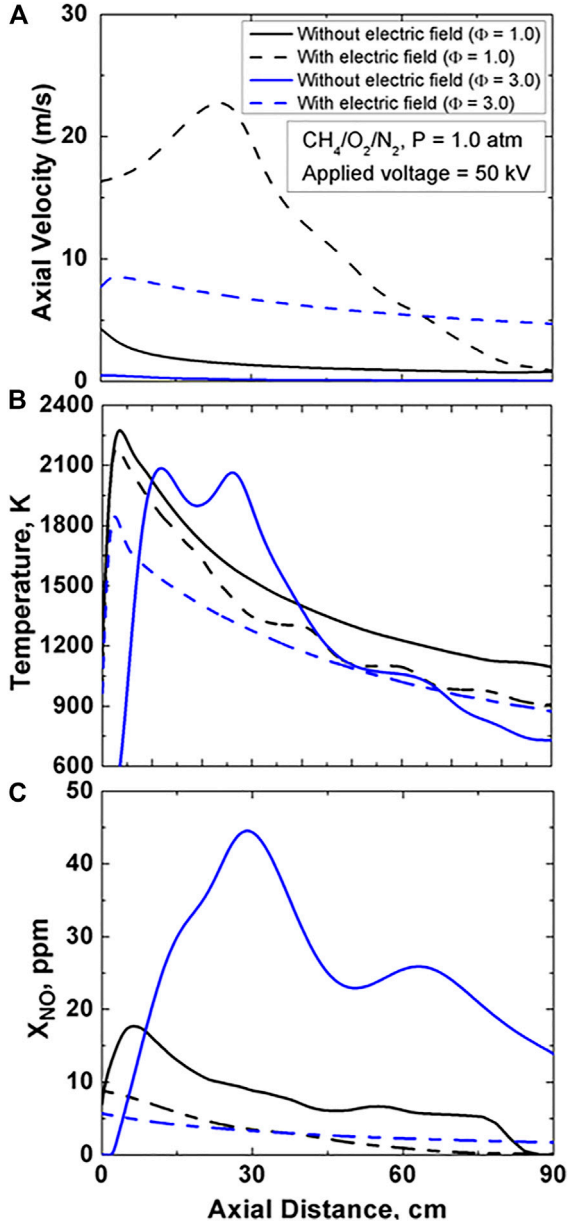

FIGURE 3
Centerline distribution of **(A)** axial velocity, **(B)** temperature, and **(C)** NO concentration with and without electric field for a premixed CH_4/air mixture with a flow rate of 3.45 slpm, 50 kV applied voltage.

2.3 Chemical kinetics

The hydrocarbon/NO_x model of Ahmed et al. (2016) consisting of 301 species and 1945 reactions is used as the chemical kinetic model for neutral species, culminated from the previous works of the authors (Santner et al., 2016). An eleven-step ionic reaction mechanism (Table 1) and associated thermodynamics and transport property from Yamashita et al. (2009) and Alquaity et al. (2017) is appended to the hydrocarbon/NO_x model. The ionic mechanism consists of six species (electrons, HCO^+, H_3O^+, $C_2H_3O^+$, CH_3^+ and $C_3H_3^+$). $C_3H_3^+$ ions are specifically considered to simulate the fuel rich flames. It should be noted that the ionic reactions are associated with chemi-ionization process and do not represent plasma breakdown by any means. The ionic mechanism has been validated by Yamashita et al. (2009) independently for a canonical configuration. The electron mobility values are obtained from Sakhrieh et al. (2005) and the Einstein

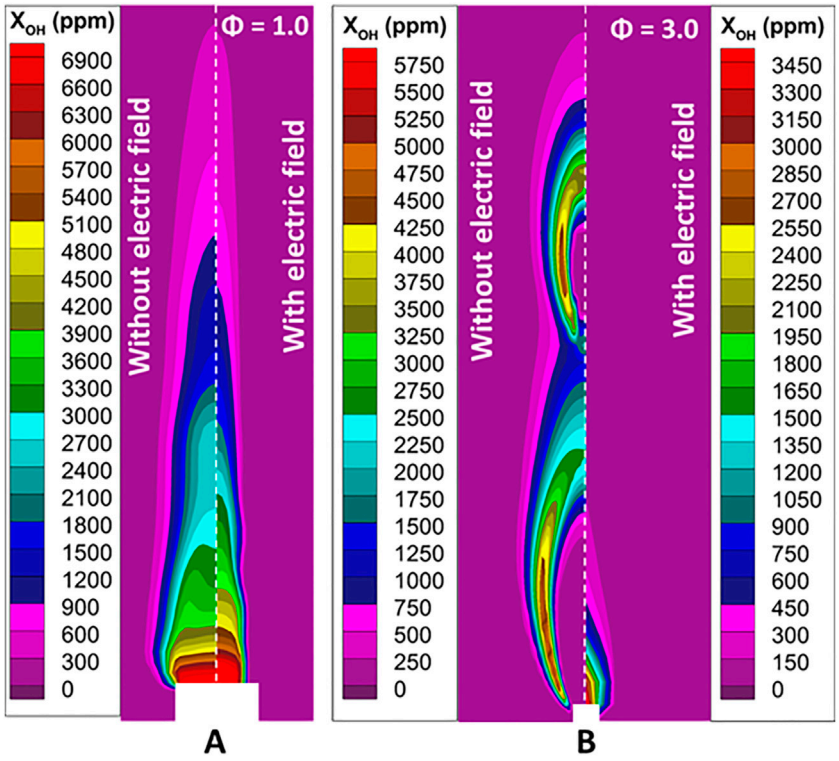

FIGURE 4
Spatial distribution of OH contours with and without electric field for **(A)** ϕ = 1.0, and **(B)** ϕ = 3.0 premixed CH_4/air with a flow rate of 3.45 slpm and applied voltage of 50 kV.

TABLE 1 Adopted ionic reactions from Yamashita et al. (2009).

Index	Reactions
1	$CH + O \rightarrow HCO^+ + e$
2	$HCO^+ + H_2O \rightarrow CO + H_3O^+$
3	$H_3O^+ + e \rightarrow H_2O + H$
4	$CH^* + O \rightarrow HCO^+ + e$
5	$H_3O^+ + C_2H_2 \rightarrow C_2H_3O^+ + H_2$
6	$HCO^+ + CH_2 \rightarrow CH_3^+ + CO$
7	$H_3O^+ + CH_2 \rightarrow CH_3^+ + H_2O$
8	$CH_3^+ + C_2H_2 \rightarrow C_3H_3^+ + H_2$
9	$C_3H_3^+ + H_2O \rightarrow C_2H_3O^+ + CH_2$
10	$CH_3^+ + CO_2 \rightarrow C_2H_3O^+ + O$
11	$CH_3^+ + e \rightarrow CH_2 + H$

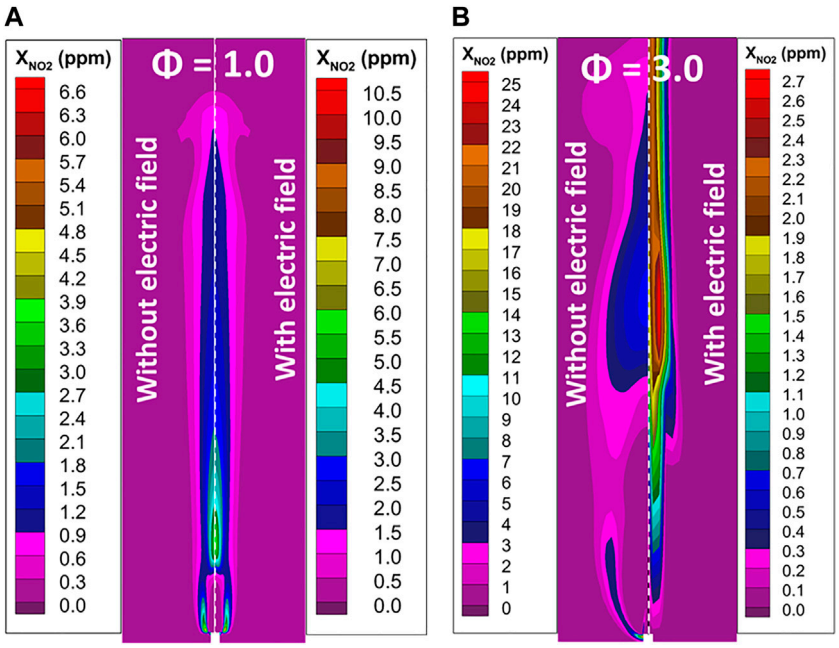

FIGURE 5
Spatial distribution of NO_2 concentration contours with and without electric field for **(A)** ϕ = 1.0, and **(B)** ϕ = 3.0 premixed CH_4/air with a flow rate of 3.45 slpm and applied voltage of 50 kV.

relationship ($D_e = \mu_e k_B T/q_e$) is used to determine the diffusivity from the mobility values.

3 Results and discussions

Figure 3 presents the center line axial velocity, temperature and NO distribution for a flow rate condition of ~ 3.45 slpm (Re = 376) for the two different equivalence ratios of ϕ = 1.0 and 3.0. These two cases are referred to as the two base case conditions. The variations due to the presence of electric field is also summarized. The presence of electric field and ionic species increases the jet velocity significantly. For ϕ = 1.0 and 3.0, the peak axial velocity is increased by a factor of ~ 6 and 17 respectively. The increase in the velocity results in stretching of the flame at ϕ = 1.0 and a complete change of the flame structure at ϕ = 3.0 (Figure 4). Among the different ions, H_3O^+ is predicted to have the maximum density, followed by HCO^+ for both cases. The predicted maximum number density of $H_3O^+_{max}$ is 8.0×10^{15} m^{-3} and 2.8×10^{15} m^{-3} and for HCO^+_{max} it is 3.2×10^{13} m^{-3} and 3.0×10^{12} m^{-3} for ϕ = 1.0 and 3.0 respectively. The resulting peak electrical body force is found to be 3875 N/m^3 and 1055 N/m^3 respectively. It is interesting to note that even though $C_3H_3^+$ ions are considered, under the very rich conditions studied, H_3O^+ are predicted to be the predominant ions. This is due to the fact that at fuel rich condition, the ionic wind promotes additional mixing of the fuel jet with the surrounding air through entrainment. The mixing allows reduction in the equivalence ratio contributing to a distinctive change in the flame structure (Figure 4B).

The temperature distribution at the centerline (Figure 3B) clearly shows a decrease in the temperature due to the ionic wind effect. The decrease in the peak temperature for ϕ = 1.0 is minimal, ~ 40 K. For the fuel rich condition, the peak temperature is lowered by ~ 230 K. Additionally, in presence of the electric field, the peak temperature shifts closer to the burner inlet with a sharper gradient downstream. The centerline NO evolution resembles the temperature distribution. The electric field is found to significantly decrease the peak NO concentration, specially under fuel rich condition.

The spatial distribution of the OH concentration contours are compared to assess the change in the flame structure due to the electric field and the associated ionic wind effect. For both fuel loading, the flame structure is radially constricted. An axial stretching is only observed for the stoichiometric fuel loading. The OH distribution under fuel rich conditions in absence of electric field show a distinctive flame structure. Even though premixed CH_4/air are injected, the extremely rich fuel loading results in a partially premixed fuel-oxidizer flame dynamics. Due to the entrainment of the chamber air to the fuel stream, the fuel-oxidizer diffuses and mixes in radial direction and establishes a flame in the periphery. The core remains fuel rich until sufficient

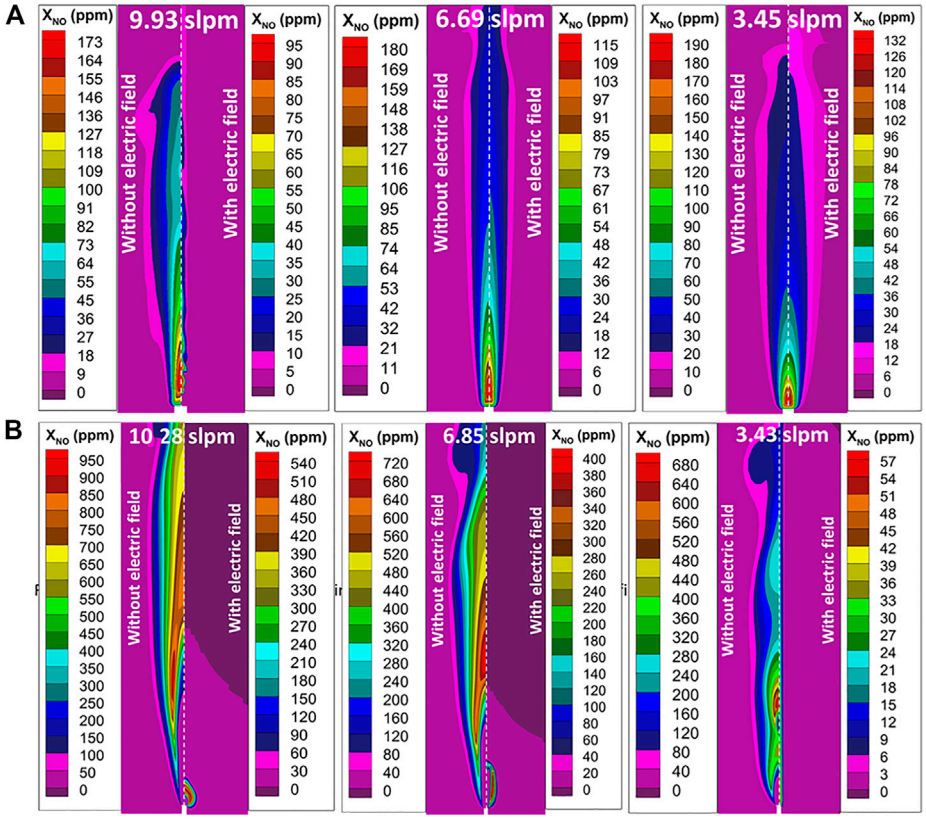

FIGURE 6
Comparisons of the NO distribution in the domain with and without electric field for premixed CH_4/air mixture under different flow rate conditions and **(A)** ϕ = 1.0, and **(B)** ϕ = 3.0.

oxidizer reaches the core region. Downstream of the burner inlet as fuel is depleted along the periphery, additional air from the surrounding gets transported into the core thereby extending the reaction zone into the core of the jet. A second peripheral reaction zone is established, as seen in the OH profile which is strictly dictated by the amount of unburnt fuel available in the jet stream. The double peak in the temperature (Figure 3B) coincides with the OH peaks in the center line. High concentration of CO overlaps with the regions of low OH in the jet core. The distribution of CH_4 concentration confirms that fuel in the jet stream is either partially oxidized to CO or completely oxidized to CO_2. In presence of electric field, the OH distribution for ϕ = 3.0 confirms that a flame structure/reaction zone close to the burner inlet is established. In addition, the OH profile looks similar to the stoichiometric fuel loading but has a smaller axial extent.

Figure 5 compares the impact of electric field on the NO_2 distribution for the base cases. Under stoichiometric fuel loading and low flow rate, electric field has minimal effect on the NO_2 emission characteristics. The spatial distribution remains fairly unaltered with a slight increase in the maximum value; less than 4 ppm. A stark contrast is observed for the fuel rich condition both in spatial distribution and peak value of NO_2. In absence of the electric field, the NO_2 is formed in the outer periphery of the flame due to radial gradient in the temperature and through NO-NO_2 recycling reactions. The peak NO_2 is decreased by a factor ~ 20 by the electric field. At the same time, the NO_2 are formed in the post combustion region downstream of the flame location.

The impact of flow rate on the NO emission for the two different fuel loadings is summarized in Figure 6. With an increase in the flow rate under stoichiometric fuel loading, the flame temperature decreases from 2,256–2,200 K under applied electric field conditions. In comparison, the ionic wind decreases the flame temperature by 40–100 K in the range of flow rate studied. For ϕ = 1.0, a change in the flow rate between 3.45–6.69 slpm minimal variations are observed. The peak NO decreases by ~ 60 ppm maintaining an almost identical spatial distribution. As the flow rate is increased to ~ 10 slpm (Figure 6A), the NO distribution is radially constricted to a very narrow central region and the peak NO is reduced by a factor of ~ 1.8. At the highest flow rate condition, a lifted flame

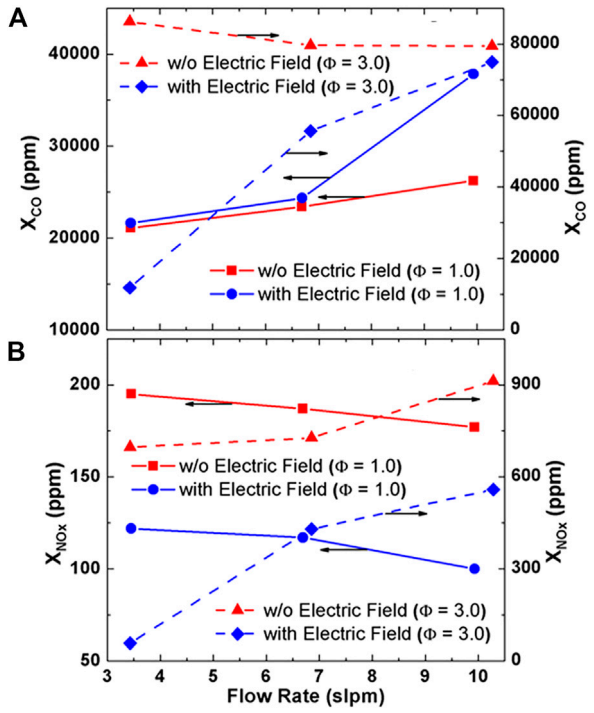

FIGURE 7
Comparisons of maximum **(A)** CO and **(B)** NO_x in the domain for different flow rate condition with and without electric field for a premixed CH_4/air mixture for two different equivalence ratio. Applied voltage 50 kV.

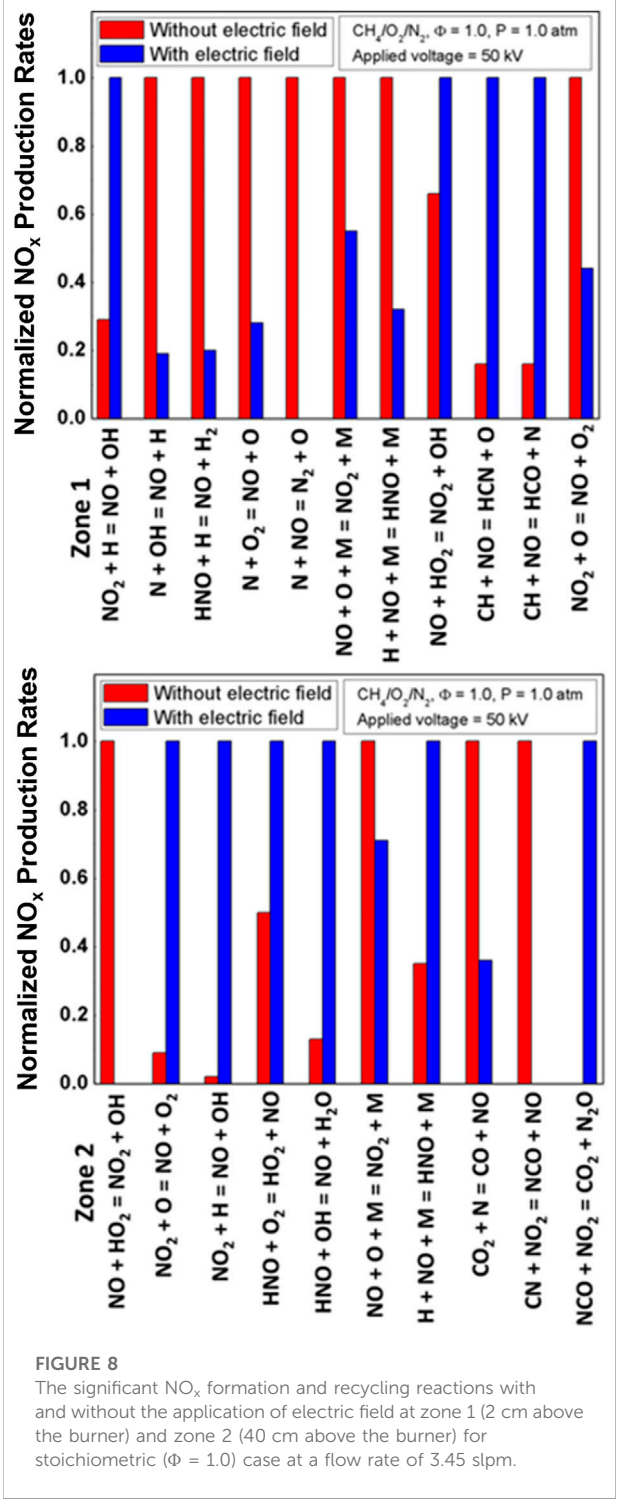

FIGURE 8
The significant NO_x formation and recycling reactions with and without the application of electric field at zone 1 (2 cm above the burner) and zone 2 (40 cm above the burner) for stoichiometric (Φ = 1.0) case at a flow rate of 3.45 slpm.

is established and maintained which is also observable in the NO contours. At higher fuel loading, the electric field allows significant decrease in the flame temperature. Over the range of flow rate simulated, the ΔT varied by ~ 160 K and 225 K for the highest and lowest flow rate respectively. Consequentially, the peak NO was found to decrease by a factor of ~ 1.8 in between 6.85 and 10.28 slpm and by ~ 12.0 at 3.43 slpm. As the electric field changes the flame structure drastically under fuel rich conditions (Figure 4B), the NO is formed in the reaction zone established very close to the burner inlet. Unlike the stochiometric condition, the NO distribution under higher fuel loading undergoes both radial and axial constriction over the entire flow rate range.

The impact of electric field on the overall emission characteristics was assessed by comparing the peak CO and total NO_x ($NO+NO_2$) prediction for the different flow rate fuel loading conditions (Figure 7). As shown in Figure 7A the peak CO concentration for $\phi = 1.0$ increases by ~ 50 ppm as the flow rate is increased. However, in presence of electric field, a non-linear trend is apparent. The sharp transition in the maximum CO concentration occurs at the highest flow rate where a lifted flame is established. The lifted flame structure increases the region of incomplete combustion and results in the increase in CO formation in the domain. In the lower flow rate range, the CO concentration increases slightly due to the fact that the radial constriction of the flame increases the gap between the burner rim (i.e., nozzle diameter) allowing some of the fuel-air mixture to bypass the reaction zone in the core. A similar

behavior was reported in Sakhrieh et al. (2005). In contrast, the rich case shows an opposite trend where CO is reduced the maximum at the lowest flow rate. However, over the entire flow rate range, the electric field is found to be effective in reducing the CO emission; allowing complete combustion to occur by mixing of the fuel rich jet stream with ambient air. The total NO_x under stoichiometric fuel loading decreases in a linear fashion and the electric field consistently decreases the maximum total NO_x by a factor of ~ 1.6 (Figure 7B). For higher fuel loading, the total NO_x is reduced by the electric field, but the emission increases with flow rate. At $\phi = 3.0$, an increase in the flow rate results in a higher flame temperature, contributing to increase NO_x production.

The influence of applied electric on the kinetics involved in NO_x formation, and NO-NO_2 interconversion was assessed by comparing the variation in the rate of formation of NO and NO_2 through the different reactions. For this purpose, two different regions in the computational domain (Zone 1: 0.17–0.27 m and Zone 2: 0.55–0.65 m above the burner surface), are selected, which represents the location of highest temperature gradients. The rates of production of NO and NO_2 by the individual reactions are volume integrated in these regions and normalized against the case without the electric field.

The comparisons for stoichiometric condition are shown in Figure 8. The decrease in flame temperature due to the application of electric field in zone 1 makes the extended Zeldovich channel ($N_2 + O = NO + N$, $N + O_2 = NO + O$, $N + OH = NO + H$) insignificant in that region. Instead, the direct NO formation channel from the recycling reaction $NO_2 + H = NO + OH$ becomes important. Besides, most of the NO in this low temperature condition in presence of electric field reacts with fuel fragments to form stable intermediates HCN and HCO. However, with the absence of electric field, most of the NO participates in direct NO-NO_2 or NO-HNO interconversion reactions.

For zone 2 downstream of the domain, where the temperature gradients are different from those at zone 1, a significantly different set of NO_x formation and recycling reactions are observed. The applied electric field changes the major NO formation path from direct oxidation ($NO_2 + OH = NO + HO_2$) to reactions with atomic hydrogen ($NO_2 + H = NO + OH$). Besides, it prompts the N_2O formation channel that is absent without ion kinetics.

4 Conclusion

A multi-dimensional multiphysics model has been developed to simulate electric-field assisted combustion process in a self-consistent fashion. The model was employed to simulate a test scale burner setup having premixed CH_4/air mixture with detailed fuel-NO_x kinetics with an ionic reaction scheme appended to it. Simulations were conducted over a range of flow rate and fuel loading condition with an applied electric potential of 50 kV to generate radial electric-fields. The emission characteristics of two major pollutant classes–CO and NO_x are investigated. The predictions show that ionic wind effects resulting from the electric field significantly increases the jet velocity and constricts the flame/reaction region both in the radial and axial direction. Lifted flames are also observed at limited cases. The flame constriction has a strong dependence on the fuel loading and flow rate conditions. Under fuel rich condition, the electric field drastically changes the flame structure by allowing mixing of the fuel stream with the surrounding oxidizing environment. A significant decrease in total NO_x is found to occur over the parametric space considered; attributed to a decrease in the flame temperature. Under fuel rich condition, the electric field is found to decrease the CO emission but *vice versa* for stoichiometric condition. The radial constriction of the flame under stochiometric fuel loading allows unburnt fuel to bypass the core reaction regime. Kinetic analysis indicates that in presence of electric field, the NO formation route shifts from Zeldovich to direct NO formation through NO_x recycling reaction and forms stable intermediates.

Data availability statement

The raw data supporting the conclusions of this article will be made available by the authors, without undue reservation.

Author contributions

JP and RG designed and built the custom test furnace. The numerical model was developed, and the simulations were run by SA, AA and TF. All the authors participated in discussing the results in the final manuscript.

Conflict of interest

JP, RG, were employed by ClearSign Combustion Corporation.

The remaining authors declare that the research was conducted in the absence of any commercial or financial relationships that could be construed as a potential conflict of interest.

Publisher's note

References

Ahmed, S., Charchi Aghdam, A., Dryer, F., and Farouk, T. (2021). Multidimensional simulations of mckenna-driven flow tube configuration: Investigating non-ideality in NO_x formation flow tube experiments. *Combust. Flame* 223, 511–524. doi:10.1016/j.combustflame.2020.10.011

Ahmed, S., Santner, J., Dryer, F., Padak, B., and Farouk, T. (2016). Computational study of NO_x formation at conditions relevant to gas turbine operation, Part 2: NO_x in high hydrogen content fuel combustion at elevated pressure. *Energy fuels.* 30, 7691–7703. doi:10.1021/acs.energyfuels.6b00421

Alquaity, A., Han, J., Chahine, M., Selim, H., Belhi, M., Sarathy, M., et al. (2017). Measurements of positively charged ions in premixed methane-oxygen atmospheric flames. *Combust. Sci. Technol.* 189, 575–594. doi:10.1080/00102202.2016.1226821

Asgari, N., Ahmed, S., Farouk, T., and Padak, B. (2017). NO_x formation in post-flame gases from syngas/air combustion at atmospheric pressure. *Int. J. Hydrogen Energy* 42, 24569–24579. doi:10.1016/j.ijhydene.2017.08.017

Belhi, M., Domingo, P., and Vervisch, P. (2010). Direct numerical simulation of the effect of an electric field on flame stability. *Combust. Flame* 157, 2286–2297. doi:10.1016/j.combustflame.2010.07.007

Belhi, M., Lee, B., Cha, M., and Im, H. (2019). Three-dimensional simulation of ionic wind in a laminar premixed Bunsen flame subjected to a transverse DC electric field. *Combust. Flame* 202, 90–106. doi:10.1016/j.combustflame.2019.01.005

Farouk, T., Farouk, B., Staack, D., Gutsol, A., and Fridman, A. (2006). Simulation of dc atmospheric pressure argon micro glow-discharge. *Plasma Sources Sci. Technol.* 15, 676–688. doi:10.1088/0963-0252/15/4/012

Kim, G., Park, D., Cha, M., Park, J., and Chung, S. (2017). Flow instability in laminar jet flames driven by alternating current electric fields. *Proc. Combust. Inst.* 36, 4175–4182. doi:10.1016/j.proci.2016.09.015

Marcum, S., and Ganguly, B. (2005). Electric-field-induced flame speed modification. *Combust. Flame* 143, 27–36. doi:10.1016/j.combustflame.2005.04.008

Ombrello, T., Won, S., Ju, Y., and Williams, S. (2010a). Flame propagation enhancement by plasma excitation of oxygen. Part I: Effects of O_3. *Combust. Flame* 157, 1906–1915. doi:10.1016/j.combustflame.2010.02.005

Ombrello, T., Won, S., Ju, Y., and Williams, S. (2010b). Flame propagation enhancement by plasma excitation of oxygen. Part II: Effects of $O_2(a^1\Delta_g)$. *Combust. Flame* 157, 1916–1928. doi:10.1016/j.combustflame.2010.02.004

Saito, M., Arai, T., and Arai, M. (1999). Control of soot emitted from acetylene diffusion flames by applying an electric field. *Combust. Flame* 119, 356–366. doi:10.1016/S0010-2180(99)00065-6

Sakhrieh, A., Lins, G., Dinkelacker, F., Hammer, T., Leipertz, A., and Branston, D. (2005). The influence of pressure on the control of premixed turbulent flames using an electric field. *Combust. Flame* 143, 313–322. doi:10.1016/j.combustflame.2005.06.009

Santner, J., Ahmed, S., Farouk, T., and Dryer, F. (2016). Computational study of NO_x formation at conditions relevant to gas turbine operation: Part 1. *Energy fuels.* 30, 6745–6755. doi:10.1021/acs.energyfuels.6b00420

Uddi, M., Jiang, N., Mintusov, E., Adamovich, I., and Lempert, M. (2009). Atomic oxygen measurements in air and air/fuel nanosecond pulse discharges by two photon laser induced fluorescence. *Proc. Combust. Inst.* 32, 929–936. doi:10.1016/j.proci.2008.06.049

Vatazhin, A., Likhter, V., Sepp, V., and Shul'gin, V. (1995). Effect of an electric field on the nitrogen oxide emission and structure of a laminar propane diffusion flame. *Fluid Dyn.* 30, 166–174. doi:10.1007/BF02029825

Vega, E., Shin, S., and Lee, K. (2007). NO emission of oxygen-enriched $CH_4/O_2/N_2$ premixed flames under electric field. *Fuel* 86, 512–519. doi:10.1016/j.fuel.2006.07.034

Yamashita, K., Karnani, S., and Dunn-Rankin, D. (2009). Numerical prediction of ion current from a small methane jet flame. *Combust. Flame* 156, 1227–1233. doi:10.1016/j.combustflame.2009.02.002

Zake, M., Turlajs, D., and Purmals, M. (2000). Electric field control of NO_x formation in the flame channel flows. *Glob. Nest Int. J.* 2, 99–108. doi:10.30955/gnj.000156

Zhang, Y., Wu, Y., Yang, H., Zhang, H., and Zhu, M. (2013). Effect of high-frequency alternating electric fields on the behavior and nitric oxide emission of laminar non-premixed flames. *Fuel* 109, 350–355. doi:10.1016/j.fuel.2012.12.083